Articles

Crystal Structure and Catalytic Mechanism of the MJ0109 Gene Product: A Bifunctional Enzyme with Inositol Monophosphatase and Fructose 1,6-Bisphosphatase Activities[†,‡]

Kenneth A. Johnson,[§] Liangjing Chen,[||] Hongying Yang,[||] Mary F. Roberts,[||] and Boguslaw Stec*[,§]

Department of Biochemistry and Cell Biology, W. M. Keck Center for Computational Biology, Rice University, Houston, Texas 77005, and Department of Chemistry, Merkert Chemistry Center, Boston College, Chestnut Hill, Massachusetts 02467

Received July 13, 2000; Revised Manuscript Received November 20, 2000

ABSTRACT: Inositol monophosphatase (EC 3.1.3.25) in hyperthermophilic archaea is thought to play a role in the biosynthesis of di-*myo*-inositol-1,1′-phosphate (DIP), an osmolyte unique to hyperthermophiles. The *Methanococcus jannaschii* MJ109 gene product, the sequence of which is substantially homologous to that of human inositol monophosphatase, exhibits inositol monophosphatase activity but with substrate specificity that is broader than those of bacterial and eukaryotic inositol monophosphatases (it can also act as a fructose bisphosphatase). To understand its substrate specificity as well as the poor inhibition by Li^+ (a potent inhibitor of the mammalian enzyme), we have crystallized the enzyme and determined its three-dimensional structure. The overall fold, as expected, is similar to that of the mammalian enzyme, but the details suggest a closer relationship to fructose 1,6-bisphosphatases. Three complexes of the MJ0109 protein with substrate and/or product and inhibitory as well as activating metal ions suggest that the phosphatase mechanism is a three-metal ion assisted catalysis which is in variance with that proposed previously for the human inositol monophosphatase.

The sole known pathway for *myo*-inositol biosynthesis is the cyclization of glucose 6-phosphate to inositol 1-phosphate by inositol-1-phosphate synthase (EC 5.5.1.4) and the dephosphorylation of inositol 1-phosphate (I-1-P)[1] by inositol monophosphatase (EC 3.1.3.25) (IMPase) (*1*−*5*). This de novo pathway is the ultimate source of *myo*-inositol for cells. In higher eukaryotes, IMPase has a crucial role in phosphoinositide signaling (*6*, *7*), where it processes the water-soluble phospholipid degradation products (inositol phosphates) produced by phospholipase C. The inhibition of human IMPase by submillimolar Li^+ (*8*) has attracted considerable attention and has made it the putative target of lithium therapy for manic depression (*9*).

This potential therapeutic significance of IMPases precipitated an intense research effort, and in the early 1990s, the human IMPase was crystallized and its structure determined (*10*). The initial papers described a homodimeric enzyme of 277 amino acids, each monomer subunit organized in a manner similar to that of pig kidney fructose 1,6-bisphosphatase (FBPase) (*11*). The structure consists of intercalated layers of β-sheets and α-helices organized into a two-domain structure analogous to the fructose bisphosphate (FBP) and adenosine monophosphate (AMP) binding domains of FBPase. Subsequent binding studies established the details of the active site where initially one, then two, and finally three metal ions were detected (*12*). Despite the detection of three metal ions in the active site (*13*), the mechanism proposed for inositol phosphoester hydrolysis relied on two metal ions to assist catalysis (*14*, *15*). Noncompetitive inhibition of IMPase by Li^+ has also been investigated with site-specific mutagenesis experiments guided by the three-dimensional structure. Both Cys218 and His217 were implicated at a site involved in Li^+ inhibition. This Li^+ site is not involved in catalysis, and the authors speculated that it may influence the binding of the metal ion at site 2, therefore hindering the release of phosphate which results in inhibition (*9*, *12*).

IMPase homologues appear to have a quite different role in hyperthermophilic microorganisms. Many of these cells

[†] B.S. acknowledges support from the W. M. Keck Center for Computational Biology via Grant 2T15LM07093. K.A.J. acknowledges support via the Hitchings-Elian fellowship from the Burroughs Wellcome fund. This work has been supported in part by Grant DE-FG02-91ER20025 (to M.F.R.) from the Department of Energy Biosciences Division.

[‡] The atomic coordinates have been deposited in the Protein Data Bank (entries 1DK4, 1G0I, and 1G0H).

* To whom correspondence should be addressed. E-mail: stec@bioc.rice.edu. Telephone: (713) 348-3346. Fax: (713) 348-5154.

[§] Rice University.

[||] Boston College.

[1] Abbreviations: FBPase, fructose 1,6-bisphosphatase; IMPase, inositol monophosphatase; I-1-P, inositol 1-phosphate; FBP, fructose 1,6-bisphosphate; F-6-P, fructose 6-phosphate.

10.1021/bi0016422 CCC: $20.00
Published on Web 01/16/2001

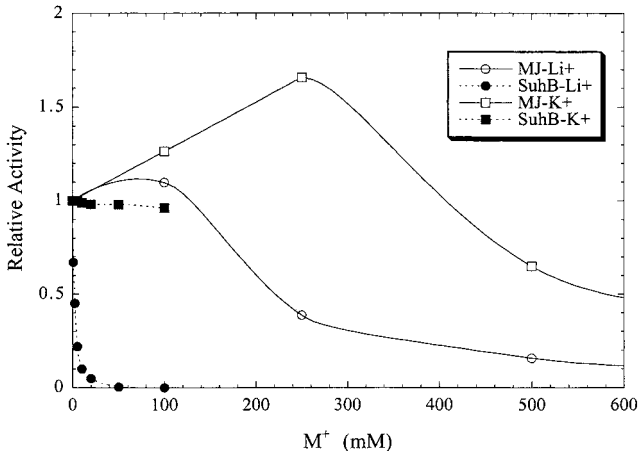

FIGURE 1: Inhibition by Li^+ and K^+ ions of IMPases MJ0109 and SuhB from *M. jannaschii* and *E. coli*, respectively. The SuhB response to monovalent cations is very similar to that of human IMPase.

do not contain phosphoinositide lipids (*16*), and the sole use of *myo*-inositol appears to be for the biosynthesis of di-*myo*-inositol-1,1′-phosphate (DIP), an unusual osmolyte (*17*, *18*). The MJ0109 gene product from the thermophilic archaeon *Methanococcus jannaschii*, first identified by its strong sequence homology to IMPases, was confirmed to be an efficient IMPase (*17*). Subsequently, it was characterized by in vitro experiments to be a bifunctional enzyme that can function as both an IMPase and FBPase (*19*). In contrast to mammalian and other bacterial IMPases, the MJ0109 enzyme is not inhibited by low concentrations of Li^+ (although this monovalent cation is much more potent than K^+; see Figure 1), even though sequence alignment programs suggest that residues corresponding to the ligands of the human enzyme exist (*17*).

We present here the results of structural studies of this novel phosphatase with sequence features similar to those of human IMPase, a structure very similar to that of pig kidney FBPase, and kinetic substrate specificity that combines traits of both enzymes (*19*). As shown in Table 1, MJ0109 has similar activities toward I-1-P and FBP. For comparison, the *Escherichia coli* IMPase cannot hydrolyze FBP and pig kidney and *E. coli* FBPase enzymes cannot hydrolyze I-1-P. Thus, the MJ0109 protein is an example of an enzyme that can catalyze, equally well, the hydrolysis of two distinct phosphomonoester substrates that in bacteria and eukaryotes are processed by separate gene products. Similar enzymes (again initially identified as IMPase homologues) were found in other hyperthermophilic organisms and were confirmed to perform double duties as IMPases and FBPases (*19*). We have crystallized three complexes of the *M. jannaschii* IMPase in the $P2_12_12_1$ space group (different from the space group found for the human enzyme). The structures include the enzyme with (i) inhibitory Ca^{2+} and I-1-P, (ii) activating Mn^{2+}, inorganic phosphate, and *myo*-inositol, and (iii) inhibitory Zn^{2+} and inorganic phosphate. The use of substrate and/or product in combination with activating or inhibitory metal ions has led to more insights into the activation process and provided a more detailed view of the IMPase catalytic mechanism. Our results also shed some light on the possible mechanism of Li^+ inhibition in the archaeal enzyme and, assuming the same mode of action, also in the human enzyme.

Table 1: Activity and Substrate Specificity of *M. jannaschii* MJ0109 Compared to *E. coli* IMPase and FBPase

	relative activity			
substrate	MJ0109[a]	*E. coli* IMPase (SuhB)[b]	*E. coli* FBPase[c]	pig kidney FBPase[c]
DL-*myo*-inositol 1-phosphate	1.00	1.00	<0.001	<0.001
myo-inositol 2-phosphate	0.15	0.03		
β-glycerol phosphate	0.80	0.50		
α-D-glucose 1-phosphate	0.68	<0.005		
2′-AMP	6.00	0.10		
pNPP	1.20	0	<0.001	<0.001
D-glucose 6-phosphate	0	<0.005		0
D-fructose 6-phosphate	0	<0.005		0
5′-AMP	0	0		
fructose 1,6-bisphosphate	1.63[d]	<0.0005	1.00	1.00
fructose 2,6-bisphosphate	0.13[e]			<0.001

[a] The specific activity for each substrate (2.5 mM) is compared to that toward DL-I-1-P (13.3 μmol min^{-1} mg^{-1}) in 10 mM $MgCl_2$ and 50 mM Tris HCl (pH 8); enzyme (0.4 μg) was added and the sample incubated for 1 min at 100 °C (data from ref *17*). [b] The specific activity for each substrate (1 mM) is compared to that for DL-I-1-P (6.9 μmol min^{-1} mg^{-1}) in 6 mM $MgCl_2$ and 50 mM Tris HCl (pH 8.0) (data from ref *38*). [c] The specific activity for each substrate (1 mM) (measured via the colorimetric inorganic phosphate assay) is compared to that for FBP (35 μmol min^{-1} mg^{-1} for the pig kidney enzyme and 20 μmol min^{-1} mg^{-1} for the *E. coli* FBPase) in 2 mM $MgCl_2$ and 50 mM Tris-HCl (pH 8.0). [d] Selectivity of MJ0109 for the phosphate on C-1 was evaluated by ^{31}P NMR spectra; the product of the incubation of the enzyme with fructose 1,6-bisphosphate was exclusively fructose 6-phosphate (*17*). [e] Since fructose 2,6-phosphate is unstable at high temperatures, the activity of MJ0109 was measured toward this substrate at 50 °C (using ^{31}P NMR to monitor reactants and products) and compared to the enzyme activity toward DL-I-1-P at 50 °C. In the 5 min assay period, there was no detectable fructose 6-phosphate produced in the absence of the enzyme; the presence of the enzyme led to selective hydrolysis of the phosphate on C-2.

MATERIALS AND METHODS

Materials. L-Inositol 1-phosphate was synthesized enzymatically using an I-1-P synthase cloned from *Archaeoglobus fulgidus* (*20*). Magnesium chloride, zinc chloride, *myo*-inositol, and PEG 8000 were purchased from Sigma Chemical Co. Tris, sucrose, and enzyme-grade ammonium sulfate were supplied by ICN Biomedicals. All other chemicals were reagent grade. Recombinant pig kidney and *E. coli* FBPase enzymes were a gift of E. Kantrowitz (Boston College).

Purification of MJ0109. Cloning the MJ0109 gene from *M. jannaschii* and overexpression of its gene product in *E. coli* were carried out as described previously (*17*). Key steps in the purification scheme include heat treatment of the crude protein (incubation at 85 °C for 30 min), followed by chromatography on Q-Sepharose fast flow and phenyl−Sepharose columns. For crystallization trials, the protein from the phenyl−Sepharose column was applied to a Sephadex G150 gel filtration column. Fractions containing I-1-Pase activity (measured with a colorimetric phosphate assay) were concentrated to a final concentration of 16 mg/mL and stored in Tris buffer [20 mM Tris-HCl (pH 8.0) with 1.0 mM EDTA].

Crystallization. Wild-type IMPase was crystallized by vapor diffusion using 10 μL hanging drops. The 5 μL enzyme solution (~16 mg/mL) was mixed with an equal volume of an 11% (w/v) solution of PEG 8000 in 50 mM Tris (pH

Table 2: Data Collection and Refinement Summary

	Ca^{2+}−I-1-P_i	Mn^{2+}−Inos−P_i	Zn^{2+}−P_i
space group	$P2_12_12_1$	$P2_12_12_1$	$P2_12_12_1$
d_{min} (Å)	2.3	2.4	2.6
no. of unique reflections	29404	26224	21614
$I/\sigma(I)$	12.2 (1.2)[a]	7.5 (1.0)[b]	8.4 (1.1)[c]
completeness (%)	98.7 (95.9)[a]	97.4 (94.5)[b]	98.3 (95.5)[c]
average redundancy	3.6 (2.3)[a]	3.0 (2.1)[b]	3.5 (2.2)[c]
unit cell dimensions (Å)	$a = 65.18$, $b = 75.89$, $c = 131.81$	$a = 68.02$, $b = 78.45$, $c = 130.05$	$a = 68.87$, $b = 78.43$, $c = 129.72$
final R_{merge}[a]	0.069 (0.41)[a]	0.090 (0.41)[b]	0.080 (0.41)[c]
free *R*-factor (calculated on 5%)			
4σ cutoff	0.235	0.256	0.257
all reflections	0.279	0.322	0.309
working *R*-factor			
4σ cutoff	0.174	0.192	0.182
all reflections	0.221	0.251	0.236
rms deviations			
bond lengths (Å)	0.014	0.014	0.014
bond angles (deg)	0.021	0.021	0.021
Ramachandran plot (%)			
most preferred	84	75	87
allowed	15	23	11
generously allowed	1	1	2
disallowed	0	0	0
model composition			
no. of water molecules	78	48	54
no. of metal ions	2	3	3
no. of substrate molecules/ product molecules	1/0	0/2	0/1

[a] Last shell (2.3−2.4 Å) data in parentheses. [b] Last shell (2.4−2.5 Å) data in parentheses. [c] Last shell (2.6−2.7 Å) data in parentheses.

7.2) with 100 mM NaCl, in the presence of 10 mM $ZnCl_2$, 10 mM $CaCl_2$, or 10 mM $MnCl_2$ in combination with inorganic phosphate, I-1-P, or *myo*-inositol with phosphate, respectively. The drops were equilibrated against the reservoir with the concentration of PEG 8000 being between 11 and 15%. Crystals appeared in a few days and grew to full size in ~3 weeks.

X-ray Data Collection. Crystals having approximate dimensions of 0.5 mm × 0.4 mm × 0.4 mm were mounted in glass capillaries directly from the crystallization wells. Diffraction data were collected at room temperature using two multiwire area detectors (Area Detector Systems, San Diego, CA), driven by a VAX ALPHA 3300 computer and linked to a Rigaku RU-200 rotating-anode generator operated at 50 kV and 150 mA using the Crystallographic Facility in the Chemistry Department of Boston College. In contrast to the apoenzyme ($P3_121$ or $P3_221$), whose crystals diffracted to only ~4 Å, all the enzyme complexes crystallized in the $P2_12_12_1$ space group and crystals diffracted to higher resolution than the apoenzyme. The data were collected to 2.3, 2.4, and 2.6 Å resolution for the Ca^{2+}, Mn^{2+}, and Zn^{2+} complexes, respectively (see Table 2). Merging of the reflections was accomplished using the software provided by Area Detector Systems. After correction for Lorentz and polarization effects, a scale factor was calculated for multiple measurements and symmetry-related reflections.

Structural Solution and Refinement. The phase problem was solved by using the molecular replacement method. The model of human inositol phosphatase was used as a probe structure (PDB entry 1AWB). The rotational as well translational searches were performed using the program Amore (*21*). The searches failed with the dimer as a model. Therefore, we used a monomer to carry out the calculation of both rotation and translation function. The self-rotation function calculations indicated that the dimer axis was confined to the $a-b$ plane. We have used this information to discriminate between the rotational solutions. The final solution was obtained in a nonconventional choice for the unit cell. The obtained solution was only marginally better than the next one, and the resulting *R*-factor was 56%. However, the resulting dimer formed by two independent solutions was similar to the dimer formed by human IMPase (1AWB). The final solution was extensively checked by rigid body refinement and subsequent REFMAC (*22*) refinements. After the correctness of the solution had been ascertainined, the coordinates were transferred into the conventional unit cell. A subsequent simulated annealing refinement with the program Xplor (*23*) lowered the *R*-factor significantly. Several macrocycles, including the manual rebuilding sessions done on the SGI workstation with the program CHAIN (*24*) and Xtalview (*25*), led to convergence. The final models were refined with the program Shelxl-97 (*26*). The inhibitory Ca^{2+} complex with the substrate (I-1-P) was refined to an *R*-factor of 0.174 at 2.3 Å resolution, while the Mn^{2+} complex was refined to an *R*-factor of 0.192 at 2.4 Å and the Zn^{2+} complex to an *R*-factor of 0.182 at 2.6 Å as calculated on reflections with $F > 4\sigma(F)$.

RESULTS AND DISCUSSION

Structure Solution, Quality, and Description of the Structure

To clarify the determinants of the broader substrate specificity and poor inhibition by Li^+, we have crystallized the MJ0109 protein. The apoenzyme crystals diffracted weakly, so we decided to crystallize the enzyme substrate

or product complex in the presence of Ca^{2+} and Zn^{2+}, metal ions that inhibit IMPase (*17*). Subsequently, we also obtained crystals with the activating metal ion Mn^{2+} and the products inorganic phosphate and *myo*-inositol. The alternate use of inhibitory and activating metal ions allowed us to trap the pre- and postcatalytic complexes of the enzyme with the substrate and both products. This process has allowed us to map the structural "intermediates" of the catalytic reaction.

The structures were determined by the molecular replacement technique as described above. Despite a medium quality of the data (low average intensity and higher R_{merge} values), the *R*-factors as well as the electron density map qualities and the geometry of the backbone and side chains indicate that the structures are reliable. The refinement statistics are presented in Table 2. All three complexes are structurally very similar. The rms deviations of the Cα positions are less than 0.6 Å, although there are some small differences between individual models, especially in the catalytic loop, which will be discussed later.

The structure is organized in five layered interleaved α-helices and *β*-sheets forming an α−*β*−α−*β*−α structure (Figure 2A). This organization of an IMPase is reminiscent of the FBPase structure as noticed previously for the structure of the human IMPase (*11*). The shortening of the N-terminal fragment eliminates the helix−turn structural motif responsible for AMP binding in FBPases. Therefore, unlike FBPase, the structure of *M. jannaschii* IMPase has two helices (residues 1−21 and 45−54) instead of three in the N-terminal region (Figure 2B). The remaining helices are very similar to the corresponding ones in human IMPase in length and in conformation with the exception of an interconnecting loop (residues 22−42) which is more similar to that in FBPase (*27*) (Figure 2C). The subsequent seven-stranded *β*-sheet contains two short helical segments in the interconnecting loops. The stretch of residues 85−92 forms a short helix whose dipole is aligned with the phosphate binding site as described previously (*28*). The remaining structure is formed by four helices (residues 159−166, 174−184, 199−212, and 242−252) and a five-stranded *β*-sheet. The helices are linkers of the individual *β*-sheet strands. The first and last helices of this fragment are located at the upper part of the subunit, while the two middle helices are internal and separate two *β*-sheets. The whole α−*β*−α motif is terminated by a short three-turn C-terminal helix (residues 242−252). The internal helices separating both *β*-sheets are of the same length as in the human enzyme, while the outer helices appear to be shorter. The first internal helix (residues 174−184) contributes its dipole to the phosphate binding site. The entire domain is reminiscent of the fructose bisphosphate binding domain of FBPase. When analyzed jointly, this entire domain has a slightly different angle as measured against the first AMP-like domain in all three enzymes (FBPase, human, and *M. jannaschii* IMPase).

The dimer interface is extensive encompassing ∼1200 Å^2. It contains contacts between the central *β*-sheet (residue 171) and a number of helices. It has only 10 hydrogen bonds compared to 22 in the human enzyme interface. One of the outer helices (residues 159−166), which in the human enzyme formed an extensive part of the interface (helix−helix contact), is shortened by 10 residues and does not interact in the *M. jannaschii* enzyme. This causes a reorganization of the dimer as described below. Despite having extensive similarities, MJ0109 also has many differences when compared to human IMPase, and in some aspects is more similar to pig kidney FBPase. The similarities and differences are described below.

Description of the Three Complexes

Ca^{2+} Complex. The structure of phosphatase cocrystallized with Ca^{2+} and I-1-P reveals two metal ions and one molecule of substrate bound at each active site of the dimer (Figure 3). The identification of the metal ion binding sites was achieved by an analysis of the difference Fourier maps. Temperature factors and the binding geometries of the moieties placed in the positive difference peaks were used as a confirmation of the identity of the metal ions. The distances to oxy ligands were in a rather wide range between 2.1 and 2.5 Å, characteristic of Ca^{2+} ions. The two metal ions are bound by residues that are homologous to those identified in metal binding in the human enzyme. The first metal ion also coordinates the ester oxygen of the I-1-P. The coordination sphere of the first metal ion appears to be a distorted octahedron formed by Asp84, Asp201, Asp81, Glu65, and two oxygen atoms of the phosphate moiety. This arrangement appears to be reminiscent of the first metal ion coordination sphere found in the structure of human IMPase with three Ca^{2+} ions (1AWB). Both Glu65 and Asp81 are bridging ligands coordinating the first as well as the second metal ion. In addition, the second metal ion is coordinated to the carbonyl of residue 83, the phosphate oxygen, and two water molecules. Hence, it also appears to be hexacoordinated. One of the water molecules can be tentatively identified as the catalytic water molecule as proposed by Bone et al. (*13*).

The inositol moiety has three hydrogen bonds formed by the 2′-, 3′-, and 4′-hydroxyl groups to the carboxyl oxygen of Asp84 (2.8 Å), the amide nitrogen of Phe175 (2.65 Å), and the guanidino nitrogen of Arg194 (3.0 Å) with distances suggesting strong and specific hydrogen bonding. Hydrogen bonds to Asp84 and Phe175 appear to be analogous to those in the human enzyme, while Arg194 replaces a bond to Glu213 in the human IMPase. Therefore, the Arg194−inositol 4′-hydroxyl interaction is specific to the *M. jannaschii* enzyme. The summary of the binding geometry is presented in Table 3.

The other important observation is a partial displacement of the catalytic loop by ∼2.5 Å from the position observed in other complexes. This observation combined with low rms deviations between the models (∼0.5 Å) underscores the intrinsic mobility of the loop as observed in the human enzyme. It may also explain the origin of different packing (space group $P3_121$) in other complexes and much lower resolution for the apo form of the enzyme. It has been proposed that removal of the metal ions causes the unwinding of this loop and its inherent disorder (*14*). The position of the loop is consistent with the presence of the two versus three metal ions seen in other complexes.

Mn^{2+} Complex. Unexpectedly, the structure of the phosphatase cocrystallized with Mn^{2+}, phosphate, and *myo*-inositol reveals three metal ions and two product molecules (Figure 4). The binding geometries of the presumed metal ions and analysis of their temperature factors positively confirmed the identity of the metal ions. The distances to

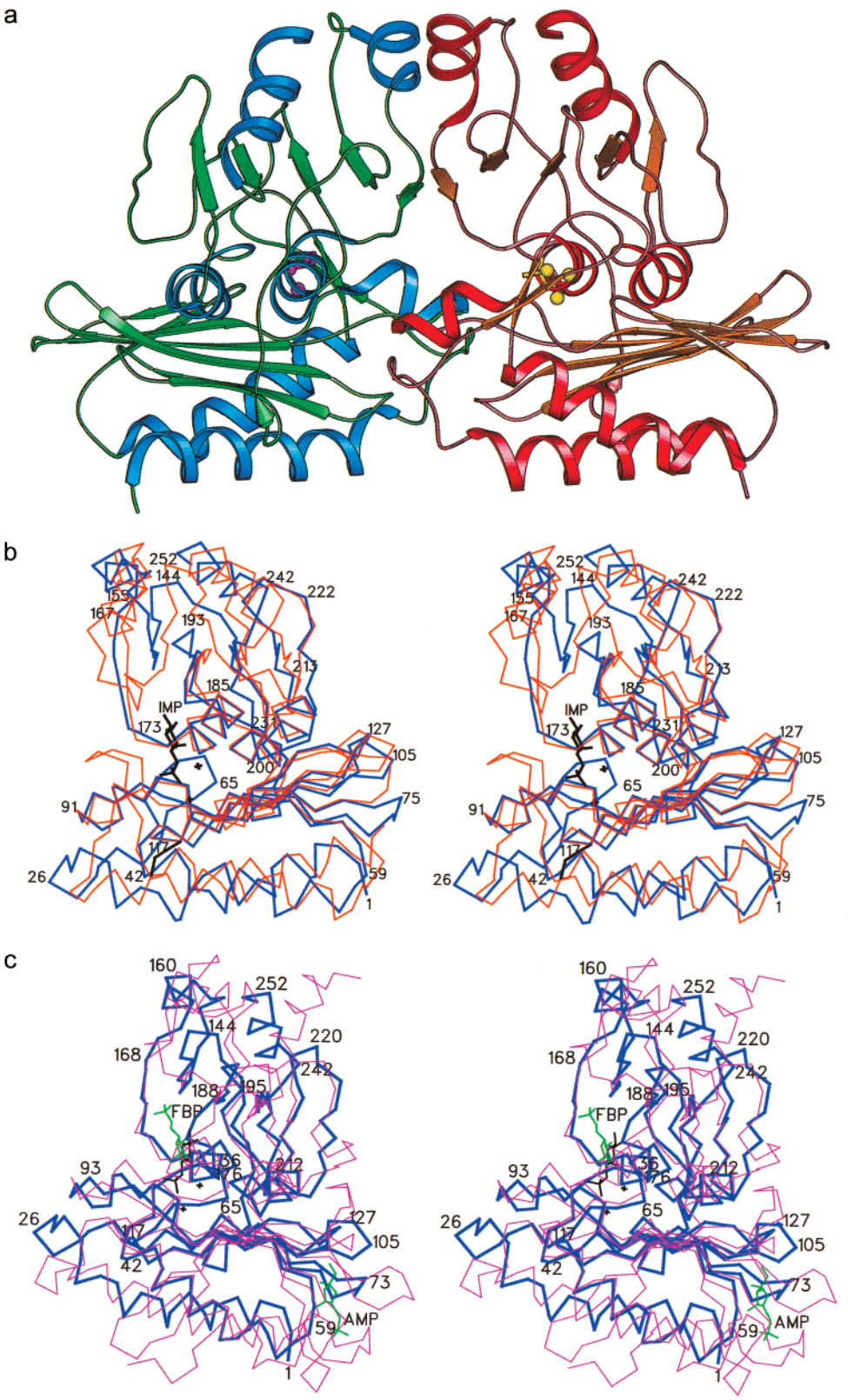

FIGURE 2: (a) Ribbon diagram of the *M. jannaschii* MJ0109 dimer. The active sites of both monomers are separated by ~30 Å with P_i present. (b) Cα representation of the MJ0109 monomer (thick blue line) superposed with human IMPase (1AWB) drawn with a thin red line (I-1-P is in black). (c) Cα representation of the MJ0109 monomer (thick blue line) superposed with pig kidney FBPase (1CQN) drawn with a thin pink line. F-6-P is depicted in green and I-1-P in black. The second F-6-P molecule occupies the AMP binding site of FBPase. This figure and all remaining figures were prepared with the program SETOR (*37*) for divergent viewing.

oxy ligands were on average shorter than in the Ca^{2+} complex and were in the range between 1.9 and 2.4 Å. Two metal

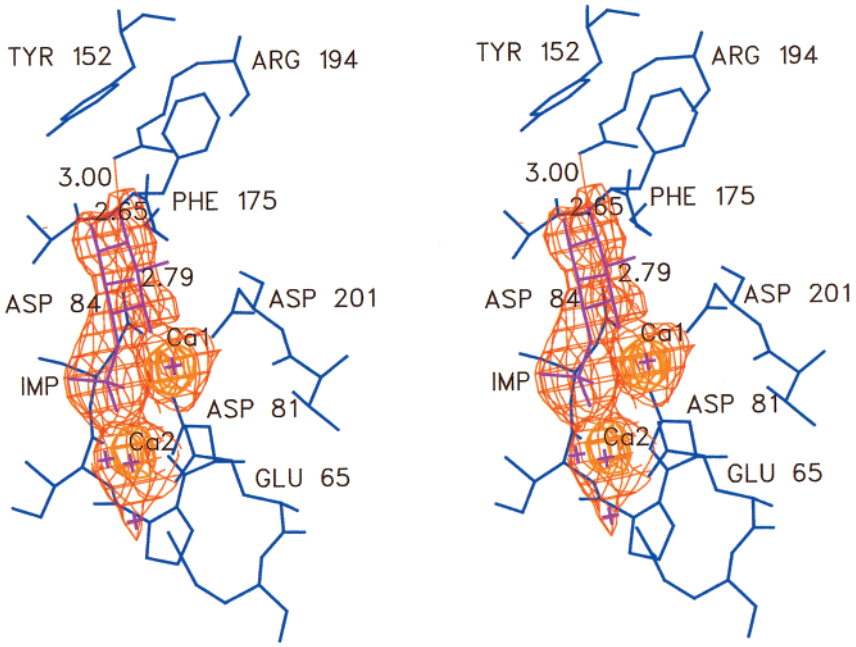

FIGURE 3: Stereodiagram of the closeup of the active site of the *M. jannaschii* phosphatase complex with inhibitory Ca^{2+} with substrate I-1-P. The $2F_o - F_c$ electron density map phased with the refined model is contoured at 1.3σ and depicted with thin red lines. The omit map contoured at the 5σ level is depicted in thick orange lines. The residues coordinating the two metal ions as well as the hydrogen bonds stabilizing the inositol moiety are labeled. The hydrogen bonds stabilizing the inositol moiety are depicted with bond lengths.

Table 3: Enzyme Active Site Interactions and Distances

structure interaction subunit	Ca^{2+} distance (Å) (A/B)	Mn^{2+} distance (Å) (A/B)	Zn^{2+} distance (Å) (A/B)
metal ions			
$Met_1 \cdots O_{\delta 1}$Asp81	2.35/2.40	2.49/1.96	2.02/1.65
$Met_1 \cdots O_{\delta 1}$Asp84	2.44/2.41	2.26/2.14	1.97/1.89
$Met_1 \cdots O_{\delta 1}$Asp201	1.98/2.00	2.06/2.10	1.96/1.95
$Met_1 \cdots O_{\gamma 1}$Glu65	2.59/2.58		
$Met_1 \cdots O_4P$	2.52/2.29		
$Met_1 \cdots O_1P$		2.19/2.14	2.71/2.42
$Met_2 \cdots O_1P$	2.33/2.22	1.83/2.13	1.75/2.11
$Met_2 \cdots O_{\delta 2}$Asp81	2.41/2.50	2.25/2.45	2.53/2.20
$Met_2 \cdots$O (Ile83)	2.39/2.29	2.20/2.25	2.11/2.09
$Met_2 \cdots O_{\gamma 1}$Glu65		2.54/2.30	1.92/1.98
$Met_2 \cdots O_{\gamma 2}$Glu65	2.26/1.89	2.33/2.88	
$Met_2 \cdots$Wat1	2.21/−	2.08/2.25	2.03/2.10
$Met_2 \cdots$Wat2	2.60/−		
$Met_3 \cdots O_2P$		2.17/1.81	1.99/1.68
$Met_3 \cdots$Wat2		2.54/2.26	1.86/2.24
$Met_3 \cdots O_{\delta 1}$Asp38		2.89/2.92	4.04/3.19
phosphate moiety			
$O_4P \cdots$N (Gly85)	3.06/3.16	2.82/2.63	3.12/3.09
$O_4P \cdots$N (Ser86)	2.79/2.96	3.26/2.68	2.85/3.20
$O_2P \cdots NH_2$ (Arg198)		2.82/2.52	−/2.87
inositol moiety			
$O2' \cdots O_{\gamma 2}$Asp84	2.51/2.60		
$O3' \cdots$N (Phe175)	2.62/2.82		
$O4' \cdots NH_2$ (Arg194)	2.96/3.15		
$O1' \cdots NH_2$ (Arg170)		2.61/2.61	
$O2' \cdots NH_2$ (Arg170)		2.60/3.02	
$O2' \cdots NH_2$ (Arg168)		3.26/2.73	
$O3' \cdots NH_2$ (Arg168)		2.70/3.43	

ions are bound very close to the positions identified as the Ca^{2+} binding sites. The difference Fourier analysis showed a third metal ion position close to the site of the third metal ion detected in the human enzyme (1AWB). Both sites 1 and 2 appear to change their coordination. The first metal ion coordination appears to be tetrahedral, with four ligands: Asp84, Asp201, and two phosphate oxygens. The second metal is coordinated by Asp84, Asp81, phosphate oxygen, Glu65, and a water molecule. The carboxylate of Glu65 has shifted and lost its bridging character and now appears to be a bidentate ligand of the metal ion in site 2. The third metal ion has less defined binding geometry with only one well-defined ligand, a phosphate oxygen. Other potential ligands are the water molecule (2.3 Å) and the more distant (~3 Å) Asp38. The resolution and quality of the electron density maps do not exclude the possibility of the second water molecule as a ligand. In the human enzyme, the third metal ion was coordinated by two water molecules that are not observed in our structure.

Along with the phosphate group detected at the active site, the *myo*-inositol moiety has also been detected in the difference Fourier maps at a distant site. This second inositol binding site is ~6 Å from the original I-1-P binding site as defined in the Ca^{2+} complex. This site is reminiscent of the frequently observed Cl^- binding site in the human enzyme. Extensive structural changes at this site create a positive environment for inositol binding. Despite only partial occupancy of the refined *myo*-inositol moiety at this site, it was possible to identify the structural determinants of the product binding. There are two arginine residues which form well-defined double hydrogen bonds to the inositol oxygens. One of them (Arg168) does not have an analogue in the human enzyme. Both arginine residues (170 and 168) reach out across the interface to the second subunit. Modeling of a substrate such as FBP shows that the 6′-phosphate moiety could reach this site once the FBP is positioned to introduce

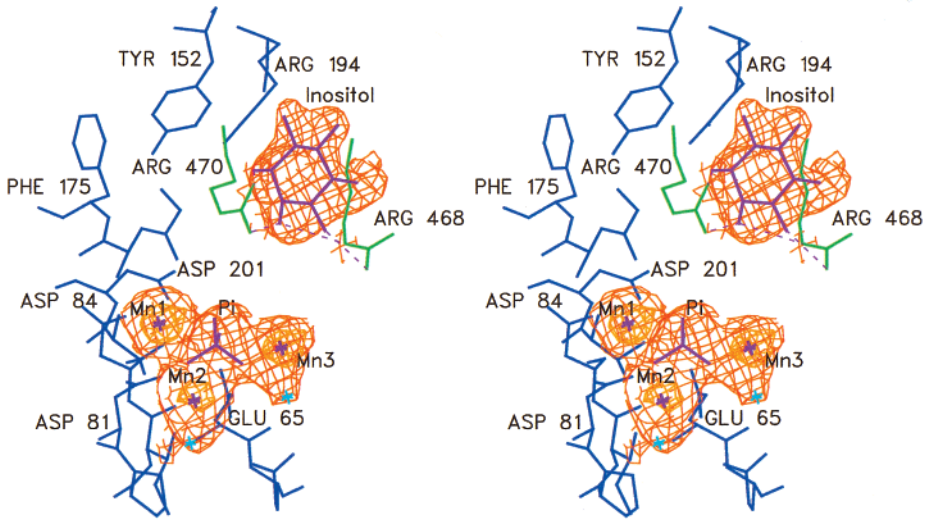

FIGURE 4: Stereodiagram of the active site of the *M. jannaschii* phosphatase complex with Mn^{2+} (an activator) and the two products *myo*-inositol and inorganic phosphate. The $2F_o - F_c$ electron density map phased with the refined model is contoured at 1.3σ and depicted with thin red lines. The omit map contoured at the 5σ level is depicted in thick orange lines. The residues of the second subunit coordinating inositol, Arg170 and Arg168, are drawn in green lines with 300 added to their residue numbers. Two water molecules directly coordinating metal ions are depicted in blue.

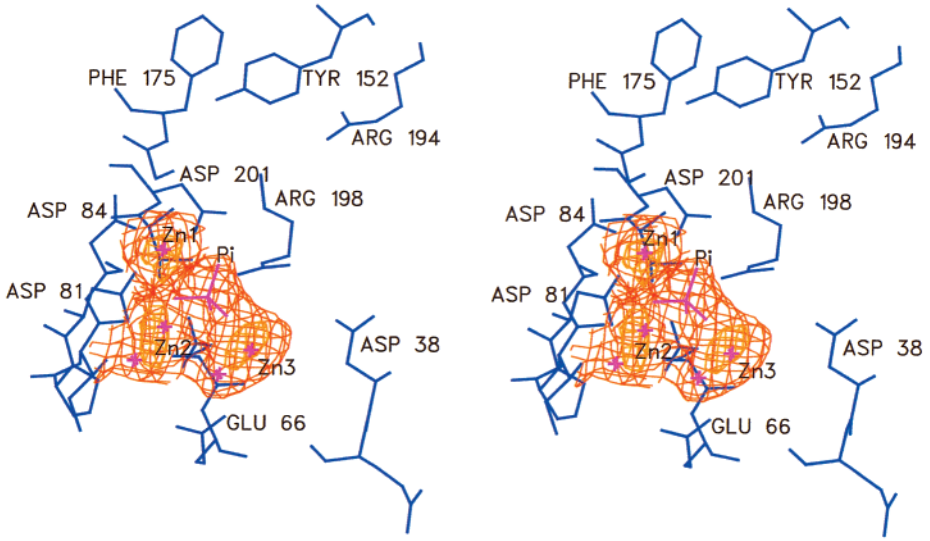

FIGURE 5: Stereodiagram of the active site of the *M. jannaschii* phosphatase complex with inhibitory Zn^{2+} and inorganic phosphate. The $2F_o - F_c$ electron density map phased with the refined model is contoured at 1.3σ and depicted with thin red lines. The omit map contoured at the 5σ level is depicted in thick orange lines. The residues coordinating the three metal ions are labeled along with residues Arg198 and Asp38 (which belongs to the catalytic loop).

1′-phosphate into the proper position for catalysis. Therefore, this site appears to be specific to the bifunctional enzyme from *M. jannaschii*. An observation that Arg170 is at a position analogous to Arg243 from pig kidney FBPase reinforces this interpretation. The experimental confirmation of the details of FBP binding must await the crystallographic determination of the complex with FBP.

Zn^{2+} Complex. The structure of phosphatase cocrystallized with Zn^{2+} and phosphate reveals once more the presence of three metal ions and one molecule of product bound at each active site of the dimer (Figure 5). The metal ions were placed on the basis of the difference Fourier maps, and their location proved to be remarkably similar to the positions of the three Mn^{2+} ions. The refined temperature factors for metal ions prove to be similar to the neighboring residues. This fact reinforces the identities of metal ions as determined by the content of the crystallization buffer. The lower resolution of this complex does not allow for the very precise determination of the bonding geometries and distances, but the apparent, refined distances were within the margin of that expected for the Zn^{2+} ions as defined by small molecule crystallography (1.9−2.3 Å). The binding geometry was very similar to that of the Mn^{2+} complex. The only exception was the lack of difference density for the inositol moiety at the distant site.

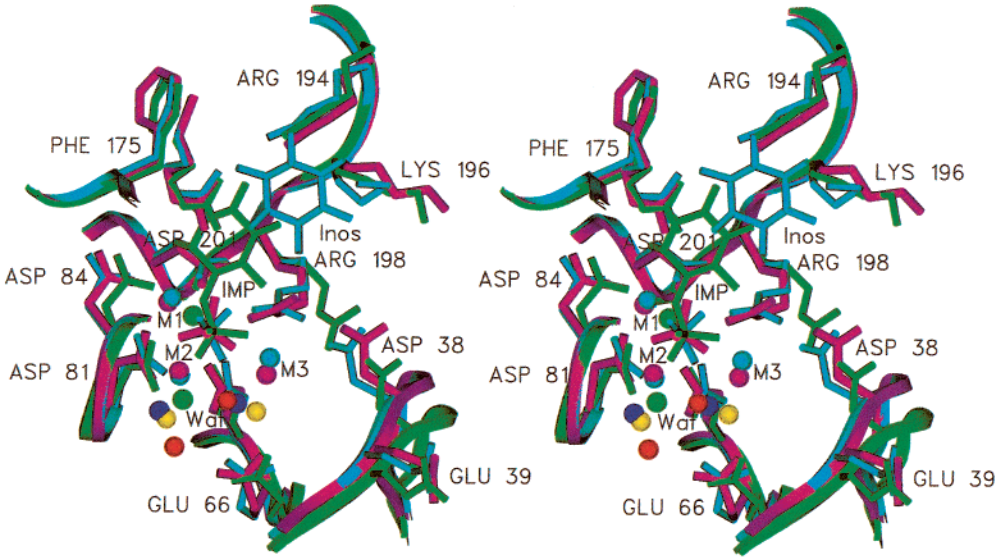

FIGURE 6: Superposition of all three complexes of MJ0109. The complex with Ca^{2+} and substrate I-1-P is depicted in green, while the model for the complex with Mn^{2+} is depicted in cyan. The inhibitory complex with Zn^{2+} is depicted in purple. Note a very good superposition of the Mn^{2+} and Zn^{2+} ions (cyan and purple spheres, respectively). Also note the displacement of the two Ca^{2+} ion positions and accompanying conformational changes of coordinating residues. Red spheres depict water molecules refined in the Ca^{2+} complex. A labeled water molecule can be tentatively identified as the water nucleophile. Yellow spheres depict water molecules refined in the Mn^{2+} complex, while blue spheres reflect waters refined in the Zn^{2+} complex. Note a movement of the catalytic loop away from the active site in the Ca^{2+} complex which is correlated with the lack of the third metal ion bound. The maximal displacement at the tip of the loop is ~2.5 Å.

Comparison of All Three Complexes. The cell dimensions provide a first glimpse into the internal differences between all enzyme complexes. The direct comparison of the unit cell dimensions shows that the Mn^{2+} and Zn^{2+} complexes must be much closer to each other than both are to the Ca^{2+} complex. The rms deviations calculated for Cα and all protein atoms of the refined structures confirm this notion. The rmsd calculated between the Cα atoms of the Mn^{2+} and Zn^{2+} complexes is ~0.4 Å, while it is ~0.7 Å for all atoms. The rmsd between the Ca^{2+} complex and both remaining complexes is around 0.6 Å for Cα positions and around 1 Å for all atoms. The origin of this divergence can be traced to the conformational transition of the catalytic loop (Figure 6). The absence of the third metal ion in the Ca^{2+}-substituted enzyme caused a ~2.5 Å shift in the position of the catalytic loop (residues 22−40). This conformational transition explains a global rotation of the dimer in the cell unit and in effect expansion of the lattice in the *c* direction.

The superposition of the active sites of the A subunit of all the complexes can be seen in Figure 6. The positions of the backbone as well of the side chain of these active sites superimposed very well except for the catalytic loop (residues 22−40). The shift of the loop precludes a direct coordination of the third metal ion by Asp38. All three metal ions refined in the structures of the Mn^{2+} and Zn^{2+} complexes superimpose very well, while the Ca^{2+} ions are shifted. This shift is reflected in the position of coordinating residues Asp81, Asp84, and Asp201. Also, residues Arg198 and Lys196 undergo the conformational transition. Both residues were previously implicated in coordinating or stabilizing the transition state which is depicted in Figure 6.

The most important observation is the change in the directionality of the phosphate group oxygens between the Ca^{2+} complex with the substrate and the Mn^{2+} complex with products. This describes especially the reversed direction of one of the phosphate oxygens which we call axial. In the Ca^{2+} complex with I-1-P, the ester oxygen is on the opposite face of the three remaining oxygens, which we call equatorial, as compared to its location in the Mn^{2+} complex with P_i and inositol. This corresponds to the reversed configuration of the phosphorus atom and defines the conformation of the pre- and postcatalytic complexes. The axial oxygen in the Mn^{2+} complex is coordinated by metal ions 2 and 3. Its position provides an approximation for an initial location of the water nucleophile. Indeed, a closer look at the Ca^{2+} complex reveals a water molecule coordinated in such a fashion that if metal ion 2 is superposed, this water position almost overlaps the axial phosphate oxygen observed in the Mn^{2+} complex.

The water molecule identified as a base is depicted in red and marked with a label in Figure 6. It is directly coordinated by metal ion 2 and Oγ of Ser86. The residue at position 86 is highly conserved across the family and was postulated to participate directly in catalysis. An additional observation is that the P_i position in the Zn^{2+} complex is more reminiscent of the pre- than of the postcatalytic orientation. This can be seen by noting that the location of one of the phosphate oxygens is reminiscent of an axial ester oxygen of I-1-P in the Ca^{2+} complex.

Comparison to the Human Enzyme: Consequences for Thermostability

Comparison of the Amino Acid Composition and Surface Accessible Areas. In recent years, a number of important papers appeared in which the structural origins of thermal stabilization were investigated (*29*−*31*). The emerging consensus is that there is no single cause for improved temperature stability, but rather, it is a combination of many

Table 4: Volume and Surface Accessible Area (SAA) for Human and *M. jannaschii* IMPase Enzymes

	human	MJ0109
volume[a] (Å^3)	47097	45464
total[a] SAA (Å^2)	21134	20809
hydrophobic SAA (Å^2)	4923	3943
polar SAA (Å^2)	6029	4648
charged SAA (Å^2)	9303	11478

[a] Calculations were performed with the program GRASP.

small contributions. However, there are a few observations that prove to be rather universal. The amino acid preferences in thermophiles constitute one of those observations. The study by Haney et al. (*31*) indicated that thermophilic proteins have increased amino acid volumes, more charged residues (especially positively charged flexible residues such as Arg or Lys), and last but not least significantly fewer polar residues (especially Ser). We have run a series of tests on the MJ0109 protein to check for those findings.

A brief look at the sequence indeed confirms most of the findings concerning the preferences in the amino acid composition. In MJ0109, there are significantly fewer Met, Thr, and Ser residues, while there are almost twice as many Tyr, Ile, Lys, Asn, and Phe residues. Surprisingly, there are no His and Gln residues present in the archaeal enzyme; this constitutes an almost 5% change in amino acid content. We have calculated the changes in molecular volume as well as solvent accessible area in the human IMPase and MJ0109. The direct comparison of the volumes and surface accessible area for the MJ0109 and the human enzyme shows that the human enzyme is larger with a larger solvent accessible area. The surface accessible area of the *M. jannaschii* enzyme is smaller by about 1000 Å^2 (a 5% decrease). This suggests that both volume and surface optimization are strategies used for temperature adaptation. The volume and surface accessible area for both enzymes are presented in Table 4.

Comparison of the Loops. The resulting structure has a significantly changed three-dimensional architecture as compared to the human IMPase (PDB entry 1AWB, Figure 2B). The *M. jannaschii* enzyme (252 amino acids) is shorter by 25 residues (the human enzyme has 277 amino acids), a difference that is mostly encompassed by the shortened loops. Five loops have been significantly altered either in length or in conformation (residues 22−42, 68−75, 152−160, and 225−234 and 10 C-terminal residues deleted), including the crucial catalytic loop (residues 22−42). However, the pattern of loop changes is more complex than a simplified picture of a shorter polypeptide.

The thermophilic enzyme has a deletion of five residues at the N-terminus. Those five residues are not included in most of the models of human IMPases deposited in the Protein Data Bank. This presumably disordered fragment must contribute to the lower temperature stability of the human enzyme. One of the first clearly resolved residues in the human enzyme, Trp5, is replaced with Trp76 and Tyr109 in the MJ0109 protein. This pattern of complementary substitutions by large space filling residues is quite characteristic throughout the protein. Yet another pattern of residue displacement is also evident. In a relatively well conserved turn just before the catalytic loop, residues Asn and Glu in the human enzyme are replaced with Arg and Lys in *M. jannaschii*. This pattern of replacement of polar but uncharged residues with positively charged flexible residues is quite common and will be discussed separately.

The first significantly changed loop is one between the first and second helices (residues 22−42). In the *M. jannaschii* enzyme, the corresponding residues contribute to the formation of the active site. However, in the human enzyme, this loop is shorter by two residues and is tilted back toward the main body of the second subunit (Figure 7A). The conformation of this loop in the MJ0109 protein is very similar to that reported for an analogous loop in pig kidney FBPase (*27*). The next significantly changed fragment is the loop encompassing residues 67−76. The corresponding loop in the human enzyme (residues 72−95) is longer by a few residues and has a loose conformation in sharp contrast to the thermophilic enzyme. In MJ0109, the loop forms an additional β-strand of the β-sheet with two tight turns at both ends (Figure 7B).

The third significantly changed loop is a deletion of 10 residues from one of the interfacial helices (residues 167−172 in FBPase). This loop is mostly responsible for the organization of the dimer. It also can be identified as a determinant of the size of the ligands that can be accommodated by the active site. A simple docking experiment with FBP shows that its binding to the human enzyme would not be possible. The shortening of loop 3 has created enough room for the 6-phosphate moiety binding.

The elongation of the fourth loop in MJ0109 seems to go against the trend of shorter loops in enzymes adapted for efficient functioning at high temperatures. However, a closer inspection reveals a pattern of substitutions which certainly reinforces the thermal stability of the enzyme. Loop 4 is elongated by five residues to compensate for the loss of 10 residues at the C-terminus. The C-terminal residues in the human enzyme penetrate the active site area, limiting the space and access to the active site. They most likely contribute to the specificity of the active site, but they also introduce some thermal instability as a loosely bound terminal fragment. The last major loop, which constituted the C-terminal fragment of the human enzyme, has been deleted. Two smaller loops add to the general optimization of the shape and space by the MJ0109. Figure 7C shows the upper domain of the MJ0109 protein superposed onto the human enzyme. It shows the pattern of substitutions of different loops discussed above.

Comparison of the Interface. The structure of the MJ0109 dimer appears to be changed with a different interface compared to the human enzyme. The surface of the interface in MJ0109 is smaller than in the human enzyme by ∼400 Å^2. Hydrophobic contacts constitute ∼50% of the total interface, while polar contacts contribute around 20% and charged contacts ∼30%. This is markedly different from the characteristics of the interface in the human IMPase. In the human enzyme, hydrophobic interactions also contribute around 50% of the total surface, but the polar (30%) and charged (20%) contacts are swapped in their mutual contributions. This indicates that adaptation to high temperature is not directly correlated with the optimization of the stability of the dimer. Additionally, the smaller interface is weakened by the loss of about 10 hydrogen bonds. The only conserved part of the interface is the crossover point around residue 171 that forms intersubunit backbone hydrogen bonds. This

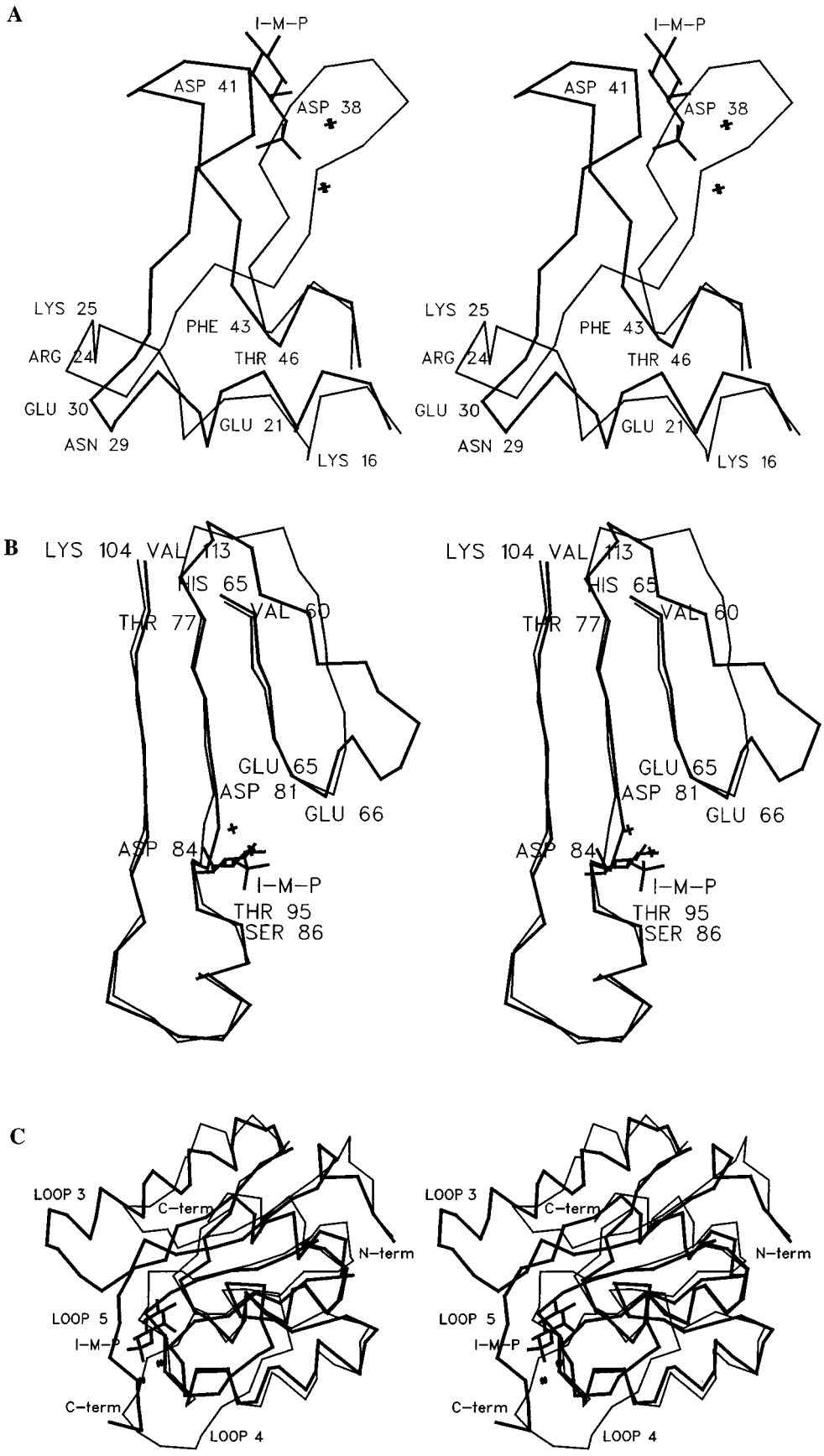

FIGURE 7: Stereodiagram of selected loops in MJ0109 (thin line) compared to human IMPase (thick line). (A) Catalytic loop 1 is shown with I-1-P and metal ions in the background. Human IMPase loop 1 has a significantly different conformation from MJ0109. Several characteristic substitutions are also labeled. (B) Loop 2 forms an additional strand in the first β-sheet, while it forms a loosely associated loop in human IMPase. (C) The "FBP domain" of MJ0109 superposed with human IMPase shows three major loop changes and two minor ones.

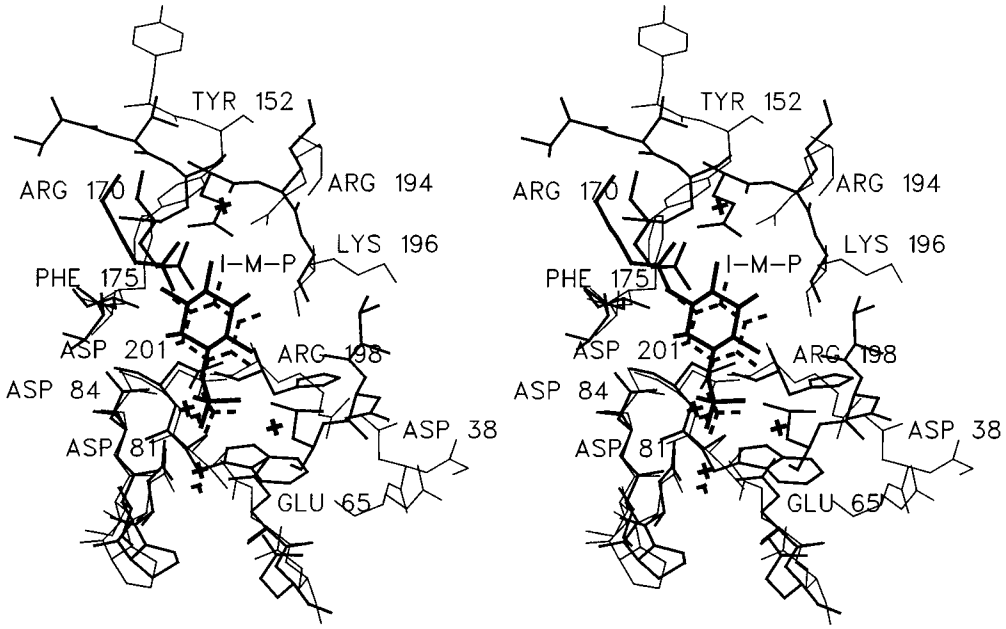

FIGURE 8: Stereodiagram of the active site of the *M. jannaschii* phosphatase complex with inhibitory Ca^{2+} (in thin lines) superposed on that of the human enzyme (1AWB) with three Ca^{2+} ions and I-1-P (thick lines). I-1-P with two metal ions found in MJ0109 is depicted in dashed lines.

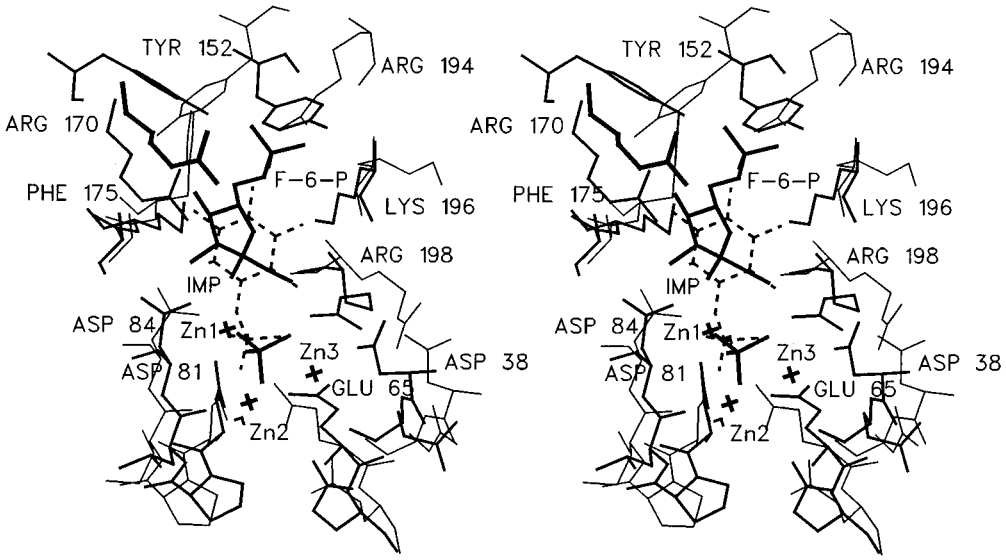

FIGURE 9: Stereodiagram of the active site of the *M. jannaschii* phosphatase complex with inhibitory Ca^{2+} (in thin lines) superposed on pig kidney FBPase (1CQN). I-1-P with two metal ions found in MJ0109 is depicted in dashed lines.

structural feature is conserved in all dimeric enzymes of the family.

The best measure of the similarity and the interface conservation of the enzymes is a rotation angle between the subunits. To superpose the second subunit of MJ0109 onto the human IMPase after superposition of the first one requires a 35° rotation along the longest axis of the dimer and a 7° rotation in the perpendicular direction. Unexpectedly, the comparison of the resulting structure (PDB entry 1DK4) showed that it is more similar to that of the recently published structure of pig kidney FBPase (1CNQ). Despite the fact that the pig kidney FBPase is a tetramer, the least-squares superposition of the second subunit also requires much less rotation (15° around the longest axis and ~5° in the other direction).

Differences with Human IMPase: What Makes MJ0109 an Efficient FBPase

To understand the specific structural differences leading to the high FBPase specific activity of the MJ0109 protein, we have compared the active site with human IMPase and pig kidney FBPase. A superposition of the active sites of the enzymes can be seen in Figures 8 and 9. Characteristically, the lower parts of the active site, which are reminiscent of the AMP domain in FBPase, are much better conserved with very few substitutions. This structural environment is responsible for the 1′-phosphate recognition and must be similar in all three enzymes. The only important conformational change involves loop 1, which has a different conformation in human IMPase. This leads to a different conformation of Asp38, a residue reported to coordinate the

third metal ion.

The upper part of the active site (Figures 8 and 9) is significantly different among all three enzymes. The MJ0109 protein is more similar to the FBPase in amino acid composition as well as in the backbone conformation of the surrounding loops. Importantly, the shortening of loop 3 has opened the active site and allowed for the creation of the 6′-phosphate group binding site. Additionally, the replacement of Gly199 in human IMPase with Arg168 in MJ0109 enhances the positive electrostatic environment for binding of the phosphate group. What also appears to be important is that Lys196 has replaced the Gly residue present in the human IMPase, allowing for the introduction of an important stabilizing residue in FBPase. Also, His217 in the human IMPase is replaced with Arg198 in MJ0109, a substitution analogous to that of Arg276 in FBPase. The latter residue was implicated in the monovalent activation of FBPases and is believed to be involved in transition state stabilization (*32*). Mutation of Arg198 in the *M. jannaschii* enzyme to His led to complete loss of IMPase activity (*17*).

In summary, the active site of the MJ0109 protein is much more open and can accommodate a wider variety of substrates. It is also more charged with the charge distribution reminiscent of the FBP binding site in FBPase. Individual amino acid substitutions contribute to the creation of high-affinity binding sites for the two phosphate moieties. Additionally, the reorganization of the loops and altered dimer interface allows for a better imitation of the FBPase active site. This is especially true for Arg170 which is homologous in position and function to Arg243, a residue proven to be necessary for the proper functioning of pig kidney FBPase (*33*).

Proposal for the Catalytic Cycle and a Possible Mode of Li^+ Inhibition

The results presented thus far can be summarized in the following statements. In the enzyme complexed with Ca^{2+} and the substrate (I-1-P), there are two metal ions bound. In the Mn^{2+} or Zn^{2+} complexes with products, there are three metal ions bound. Therefore, binding of the third metal ion is weaker and not necessarily correlated with substrate binding. However, the human IMPase model (1AWB) and the experimental procedures leading to this particular structure indicate that it is possible to have the substrate bound to the enzyme in the presence of three metal ions, but it requires a much higher concentration of the metal ions (200 mM Ca^{2+} acetate). The differences in metal ion content as well as their coordination provide some needed clues for understanding in detail the catalytic cycle.

Bone et al. (*14*) proposed that the catalytic reaction is best described as a two-metal ion assisted catalysis. The third metal ion site was described as spurious. They also noticed significant similarities between the mechanisms proposed for alkaline phosphatase (*34*) and FBPase for which the two metal ion catalytic cycles had been proposed (*35*). More recently, the descriptions of the catalytic cycles for those enzymes were amended, and it has been proven that alkaline phosphatase (*36*) as well as FBPase operates through three-metal ion assisted catalytic cycles (*27*).

We have reexamined the evidence gathered by Bone et al. (*13*, *14*) and concluded that it is fully compatible with

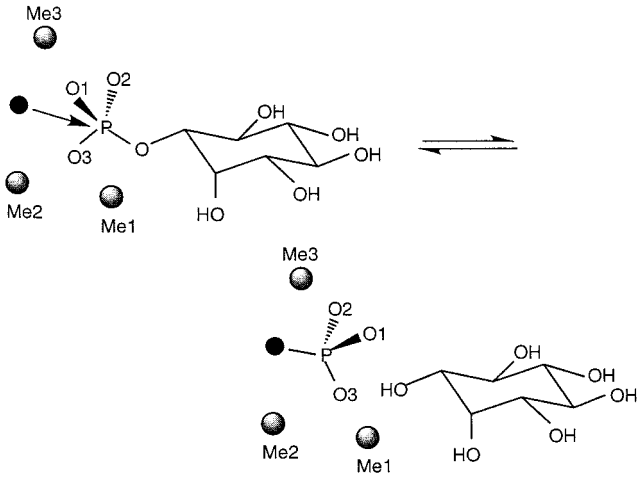

FIGURE 10: Schematic of the proposed reaction mechanism for the IMPases. Metal ions 1 and 2 are postulated to be responsible for substrate binding and stabilization of the trigonal arrangement of the intermediate, while metal ions 2 and 3 are postulated to be responsible for the positioning of the water nucleophile and release of phosphate.

the following scenario suggested by our work with the archaeal IMPase. Initially, two metal ions are needed for the creation of the appropriate substrate binding site. The substrate usually carries with it a third metal ion whose binding to the enzyme is weaker and not cooperative. The third metal ion appears to be in an appropriate position to participate in the creation of the water nucleophile. Mutation in FBPase and human IMPase of analogous residues at the catalytic loop resulted in severely impaired enzymes. The water molecule bound by two metal ions (sites 2 and 3) appears to have the right environment for deprotonation and the creation of the hydroxide that could serve as the primary nucleophile. This nucleophilic water molecule would approach the phosphate in an in-line attack. Collapse of the pentagonal intermediate would cause phosphate hydrolysis and invert the phosphate configuration. After hydrolysis, which consumes the negatively charged hydroxide, the binding of the third metal ion would become weaker. This metal ion would no longer be essential and could take a remote position detected in the crystal structures. It could also be released, neutralizing the phosphate. Two metal ions, at sites 1 and 2, stabilize the trigonal geometry of the transition state in the same way as they do in alkaline phosphatase (*36*). The metal at site 1 should serve to stabilize the developing negative charge on the phosphate oxygen. The residues coordinated by it are well equipped to provide a proton necessary for the release of phosphate. The overall model of the single-step hydrolysis of phosphate groups by IMPases and related enzymes is presented in Figure 10.

The scenario described above offers an explanation for why only two metal ions were detected upon soaking the crystals containing Mn^{2+} with phosphate, and why binding of the third metal ion is not cooperative. Its binding is weak and only weakly correlated with substrate and/or product binding. Consistent with this picture is the observation that in the human IMPase three metal ions were observed with bound Cl^- ion, while soaking the crystal with inorganic phosphate expelled the third metal ion. However, it is possible to bind all three metal ions to the IMPase with substrate or product present as our work and that of Ganzhorn

et al. (1AWB) show. Therefore, the suggested role of the mobile catalytic loop (residues 22−42) is most likely in positioning the third metal ion. This observation is very much in agreement with the results of Choe et al. (*27*), who implicated that loop in catalysis and the transmission of the AMP allosteric signal and inhibition of pig kidney FBPase.

The prevailing notion for the mechanism of Li^+ inhibition of IMPase is that the Li^+ ion substitutes for one of the Mg^{2+} ions and hinders product release (*14*). However, if we assume that the appropriate constellation of the residues on the catalytic loop plays a role in binding and creation of the water nucleophile, a tempting possibility is to implicate this loop in Li^+ inhibition. The loop has a different conformation in the MJ0109 enzyme and in the human enzyme that is clearly correlated with different Li^+ inhibition. The archaeal enzyme is not inhibited by low concentrations of Li^+, while the human enzyme is inhibited by Li^+ at submillimolar concentrations. We are presently working on experiments to test this hypothesis.

SUMMARY

In this report, we have presented the X-ray crystallographic determination of the *M. jannaschii* MJ0109 gene product, a bifunctional enzyme with dual IMPase and FBPase activities (*19*). We have analyzed the structure and discussed the structural features that make it an efficient IMPase and the structural details that allow it to also function as an FBPase. The overall adaptation of an IMPase to high temperatures appears to be aided by shortening of loops and making them less flexible. There are also differences in overall shape and surface accessible area for different classes of amino acids in this thermostable enzyme. Finally, the analysis of metal ions and substrate or product binding has allowed us to propose an amended catalytic mechanism based on three-metal ion assisted catalysis. The analysis of structural differences between human and archaeal IMPase enzymes together with consideration of the role of the third metal ion has allowed us to suggest the possible mode of Li^+ inhibition in the human enzyme and correlate the structural changes to the diminished sensitivity to Li^+ of the thermophilic enzyme.

ACKNOWLEDGMENT

We thank Dr. Evan Kantrowitz (Boston College) for the *E. coli* and pig kidney FBPase enzymes.

REFERENCES

1. Chen, I.-W., and Frixos, C. C. (1965) *J. Biol. Chem. 241*, 2194−2199.
2. Chen, I.-W., and Frixos, C. C. (1966) *J. Biol. Chem. 240*, 3507−3512.
3. Eisenberg, F., Jr., and Ranganathan, P. (1987) *Methods Enzymol. 141*, 127−143.
4. Loewus, F. A. (1990) *Inositol Metabolism in Plants*, pp 13−19, Wiley-Liss, Inc., New York.
5. Majerus, P. W. (1992) *Annu. Rev. Biochem. 61*, 225−250.
6. Berridge, M. J., and Irvine, R. F. (1989) *Nature 341*, 197−205.
7. Rana, R. S., and Hokin, L. E. (1990) *Physiol. Rev. 70*, 115−161.
8. Hallcher, L. M., and Sherman, W. R. (1980) *J. Biol. Chem. 255*, 10896−10901.
9. Gore, M. G., Greasley, P., McAllister, G., and Ragan, C. I. (1993) *Biochem. J. 296*, 811−815.
10. Bone, R., Springer, J. P., and Atack, J. R. (1992) *Proc. Natl. Acad. Sci. U.S.A. 89*, 10031−10035.
11. Zhang, Y., Liang, J. Y., and Lipscomb, W. N. (1993) *Biochem. Biophys. Res. Commun. 190*, 1080−1083.
12. Pollack, S. J., Knowles, M. R., Atack, J. R., Broughton, H. B., Ragan, C. I., Osborne, S., and McAllister, G. (1993) *Eur. J. Biochem. 217*, 281−287.
13. Bone, R., Frank, L., Springer, J. P., Pollack, S. J., Osborn, S., Atack, J. R., Knowles, M. R., McAllister, G., Ragan, C. I., Broughton, H. B., Baker, R., and Fletcher, S. R. (1994) *Biochemistry 33*, 9460−9467.
14. Bone, R., Frank, L., Springer, J. P., Pollack, S. J., Osborn, S., and Atack, J. R. (1994) *Biochemistry 33*, 9468−9476.
15. Pollack, S. J., Atack, J. R., Knowles, M. R., McAllister, G., Ragan, C. I., Baker, R., Fletcher, S. R., Iversen, L. L., and Broughton, H. B. (1994) *Proc. Natl. Acad. Sci. U.S.A. 91*, 5766−5770.
16. Koga, Y., Morii, H., Akagawa-Matsushita, M., and Ohga, M. (1998) *Biosci., Biotechnol. Biochem. 62*, 230−236.
17. Chen, L., and Roberts, M. F. (1998) *Appl. Environ. Microbiol. 64*, 2609−2615.
18. Chen, L., Yang, H., Wolff, S., Hensel, R., Huber, H., Stetter, K., and Roberts, M. F. (2000) *Appl. Environ. Microbiol.* (submitted for publication).
19. Stec, B., Yang, H., Johnson, K. A., Chen, L., and Roberts, M. F. (2000) *Nat. Struct. Biol. 7*, 1046−1050.
20. Chen, L., Zhou, C., Yang, H., and Roberts, M. F. (2000) *Biochemistry 39*, 12415−12423.
21. Navaza, J. (1994) *Acta Crystallogr. A50*, 157−163.
22. Murshudov, G. N., Vagin, A. A., and Dodson, E. J. (1997) *Acta Crystallogr. D53*, 240−255.
23. Brünger, A. T. (1992) *X-PLOR, Version 3.1*, Yale University Press, New Haven, CT.
24. Sack, J. S. (1988) *J. Mol. Graphics 6*, 244−245.
25. McRee, D. E. (1999) *J. Struct. Biol. 125*, 156−165.
26. Sheldrick, G. M., and Schneider, T. R. (1997) *Methods Enzymol. 277*, 319−343.
27. Choe, Y. Z., Poland, B. W., Fromm, H. J., and Honzatko, R. B. (1998) *Biochemistry 37*, 11441−11450.
28. Copley, R., and Barton, G. J. (1994) *J. Mol. Biol. 242*, 321−329.
29. Thompson, M. J., and Eisenberg, D. (1999) *J. Mol. Biol. 290*, 595−604.
30. Szilagyi, A., and Zavodszky, P. (2000) *Structure 8*, 493−504.
31. Haney, P. J., Badger, J. H., Buldak, G. L., Reich, C. I., Woese, C. R., and Olsen, G. J. (1999) *Proc. Natl. Acad. Sci. U.S.A. 96*, 3578−3583.
32. Zhang, Y., Villeret, V., Lipscomb, W. N., and Fromm, H. J. (1996) *Biochemistry 35*, 3038−3043.
33. Stec, B., Abraham, R., Giroux, E., and Kantrowitz, E. R. (1996) *Protein Sci. 5*, 1541−1553.
34. Kim, E. E., and Wyckoff, H. W. (1991) *J. Mol. Biol. 218*, 449−464.
35. Villeret, V., Huang, S., Zhang, Y., and Lipscomb, W. N. (1995) *Biochemistry 34*, 4307−4315.
36. Stec, B., Holtz, K., and Kantrowitz, E. R. (2000) *J. Mol. Biol. 299*, 1303−1311.
37. Evans, S. V. (1993) SETOR: hardware lighted three-dimensional solid model representation of macromolecules, *J. Mol. Graphics 11*, 134−138.
38. Chen, L., and Roberts, M. F. (2000) *Biochemistry 39*, 4145−4153.

BI0016422